CALCULATING VEGETATION INDEX BASED ON THE UNIVERSAL PATTERN DECOMPOSITION METHOD (VIUPD) USING LANDSAT 8

Xiaojun She[a,b], Lifu Zhang[a], Muhammad Hasan Ali Baig[a,b] ,Yao Li[a,b]

[a]Institute of Remote Sensing and Digital Earth, Chinese Academy of Sciences, Beijing, China
[b]University of Chinese Academy of Sciences, Beijing, China

ABSTRACT

This study introduced the vegetation index based on the universal pattern decomposition method (VIUPD) and then applied on a new sensor—Landsat 8 Operational Land Imager (OLI). VIUPD is a valuable sensor-independent spectral analysis method. Each pixel is described as the linear mixture of standard spectral patterns for water, vegetation, soil and supplementary patterns included when necessary. In the present paper, processing procedure about the data acquisition, radiometric calibration and atmospheric correction have been elaborated. The normalized reflectance (P) of four standard samples resampled to OLI has been listed. For validation of the results, Normalized Difference Vegetation Index (NDVI) and VIUPD have been calculated for comparison. The results showed that VIUPD is more sensitive to the vegetation amount change even in the high vegetation coverage, while the NDVI is more rapidly saturated in high vegetation cover area. In addition, VIUPD is more sensitive to the soil background than NDVI.

Index Terms— VIUPD, UPDM, Landsat, Operational Land Imager, sensor independent.

1. INTRODUCTION

Identifying the state of vegetation over a wild range and long-term is important in regional and global modeling, ecological monitoring and climate change detection[1]. Remote sensing data obtained using satellite instruments, offer the potential of measuring vegetation status across a wide area of spatial and temporal scales. Vegetation indices are the simplest and most efficiently way to evaluate the information of vegetation from remote sensing data. The traditional vegetation index such as Normalized Difference Vegetation Index (NDVI) was put forward to use the usual satellite red and near-infrared bands. In another word, they relies on the sensors so it will has limits when two or more sensors fusion or compared. VIUPD is a sensor independent vegetation index based on the Universal Pattern Decomposition Method (UPDM) which can be applied on both multispectral data and hyperspectral data. Pattern decomposition coefficients for each pixel contain almost all the sensor-derived information. More importantly, the VIUPD is independent of sensors[2]. Many researchers demonstrated the applications of VIUPD by using different sensors, such as TM, ETM+, MODIS and hyperspectral sensors like Hyperion and CHRIS[2, 3].

Landsat program has been dedicated to sustaining data continuity for nearly four decades[4, 5] and accumulate rich high spatial resolution and multi-spectrum remote sensing images[6]. The continuous Landsat data source provides long-term observation for global change, especially on land cover change detection and vegetation phenology [6-9]. Lately the launching of Landsat 8 injected new blood into this big and ancient family to make it continually serve for researchers to earth observation. Since the Landsat 8 is a new sensor, the independent vegetation index—VIUPD has not been used on the OLI onboard the Landsat 8. The objective of this paper is to demonstrate how to get the VIUPD parameters for Landsat 8 data.

2. METHOD

VIUPD is based on the universal pattern decomposition method (UPDM)[10]. UPDM has improved the pattern decomposition method (PDM) to make the parameters independent on sensors. The principle of UPDM is based on that each pixel measured by the sensor can be decomposed into three standard spectral elements which are the water, vegetation and soil as the following equation (1) described.

$$R(i) \to C_w \cdot P_w(i) + C_v \cdot P_v(i) + C_s \cdot P_s(i) + C_4 \cdot P_4(i) \quad (1)$$

Where *R(i)* is the reflectance of band *i* for each pixel. C_w, C_v, C_s are the decomposition coefficients, in other words, they stand for the abundance for each element. P_w, P_v, P_s are the normalized reflectance of standard samples which are the water, vegetation, soil and supplementary yellow leaf. Three components can cover about 95.5% information of spectral reflectance. Adding on the fourth supplement component will reduce the error.

Each *P* can be got as follows:

$$P_k(\lambda) = R_k(\lambda)\frac{\int d\lambda}{\int R_k(\lambda)d\lambda} \quad (k = w, v, s, 4) \qquad (2)$$

Where, λ is the wavelength, k contains the four standard samples which are the water, vegetation, soil and supplementary yellow leaf. If we integral for P in the full-range wavelength, no matter for which sample we can get:

$$\int P_k(\lambda) = \int d\lambda \qquad (3)$$

That is to say, P has normalized on the wavelength. Because of the equation (3), the integral for equation (1) can be shown as:

$$\int R(i) \to C_w \cdot \int P_w(i) + C_v \cdot \int P_v(i) + C_s \cdot \int P_s(i) + C_4 \cdot \int P_4(i)$$
$$\to (C_w + C_v + C_s + C_4)\int d\lambda \qquad (4)$$

Or
$$C_w + C_v + C_s + C_4 = \frac{\int R d\lambda}{\int d\lambda} \qquad (5)$$

The equation (5) represents the sum of total reflectance; even a supplementary pattern is included. When the satellite bands are more than standard samples, we'd better use the least square method to get C to obtain the least error:

$$C = (P^T P)^{-1} P^T R \qquad (6)$$

Since decomposition coefficients (C_w, C_v, C_s, C_4) are independent of sensors, we utilized a vegetation index based on the universal pattern decomposition method.

$$VIUPD = \frac{C_V - aC_S - C_4}{C_W + C_V + C_S} \qquad (7)$$

The soil pattern factor a is recommended as 0.1 by Zhang[10].

3. DATA

Landsat 8 took Landsat 5's orbit after launching on February 11, 2013, continuing the Landsat program's long legacy. After the fast development of satellite observation during the past decades, Landsat 8 made a great change in the spectral bands (see in table 1) and made a better balance of signal and noise (http://landsat.usgs.gov/landsat8.php). The biggest change occurs in OLI band 5 (0.845–0.885μm) to exclude a water vapor absorption feature at 0.825μm obtained in ETM+ near infrared band (0.775–0.900μm). Besides, two new bands are added in the OLI: deep blue band (band 1: 0.433 - 0.453) which provides the ocean color observations in coastal zones and a shortwave infrared band (band 9: 1.360 - 1.390) to detect the cirrus.

The Landsat 8 products can be obtained from the USGS website (http://earthexplorer.usgs.gov/). One Landsat 8 image (LC81230322013132LGN02) contained Beijing, China was been downloaded in this paper. From its name, we can easily read its Path/Row and acquisition data. The downloaded data is level 1T data which have only been geometrically corrected. The remaining process contains radiometric calibration to the radiance and atmospheric correction to the surface reflectance and to calculate the vegetation indices based on the Landsat scene.

Table 1. Bands and wavelength of Landsat 8 Operational Land Imager (OLI) and Thermal Infrared Sensor (TIRS)

Bands	λ(μm)
Band 1- Coastal aerosol	0.433 - 0.453
Band 2- Blue	0.450 - 0.515
Band 3- Green	0.525 - 0.600
Band 4- Red	0.630 - 0.680
Band 5- Near Infrared	0.845 - 0.885
Band 6- SWIR 1	1.560 - 1.660
Band 7- SWIR 2	2.100 - 2.300
Band 8- Pan	0.500 - 0.680
Band 9- Cirrus	1.360 - 1.390
Band 10- TIRS 1	10.60 - 11.19
Band 11-TIRS 2	11.50 - 12.51

3.1 Radiometric Calibration

First of all, radiometric calibration is needed to rescale the unsigned integer format to radiance using radiometric rescaling coefficients provided in the product metadata file (.MTL file).

$$L_\lambda = \mathrm{M_L} Q_{cal} + A_L \qquad (8)$$

where:
L_λ is TOA spectral radiance (Watts/(m2 * srad * μm)); M_L is Band-specific multiplicative rescaling factor from the metadata (RADIANCE_MULT_BAND_x, where x is the band number); A_L is Band-specific additive rescaling factor from the metadata (RADIANCE_ADD_BAND_x, where x is the band number); Q_{cal} is Quantized and calibrated standard product pixel values (DN).

3.2 Atmospheric correction

To extract quantitative information from the Landsat OLI imagery accurately, atmospheric correction is a necessary step. 6S (Second Simulation of the Satellite Signal in the Solar Spectrum) approach is been used for this purpose. The 6S is a basic radiative transfer code used for calculation of lookup tables in the MODIS atmospheric correction algorithm[11]. It enables accurate simulations of satellite or plane observation, accounting for elevated targets, use of anisotropic and lambertian surfaces and calculation of gaseous absorption. Since the previous TM on board Landsat 5 and ETM+ on board Landsat 7 which have been released the surface reflectance products used the MODIS/6S methodology[12], it will helpful to maintain the data continuity of Landsat series data.

3.3 Calculate the VIUPD

Since we want to apply the VIUPD to Landsat 8 data, firstly we should measure the standard samples including

vegetation, water, soil and yellow leaf as the standard spectral patterns. Then normalize the standard spectrum according to equation 2. Thirdly, resample these continuous spectral to the Landsat 8\OLI sensor. The other sensor TIRS onboard the Landsat 8 is not used for our resample because the wavelengths of TIRS are not the response range of vegetation. What's more, the first band which has been designed to study the coastal aerosol and the band 9 which has been used for the cirrus research and the panchromatic band are not involved in the resample process.

The result of P is as follows:

$$P_w = \begin{bmatrix} 3.2877 \\ 2.7790 \\ 1.4766 \\ 0.7895 \\ 0.2371 \\ 0.2114 \end{bmatrix}, P_v = \begin{bmatrix} 0.1698 \\ 0.4097 \\ 0.1712 \\ 2.3318 \\ 0.9666 \\ 0.3629 \end{bmatrix}, P_s = \begin{bmatrix} 0.5402 \\ 0.7741 \\ 0.9235 \\ 0.9703 \\ 1.2467 \\ 1.1839 \end{bmatrix}, P_4 = \begin{bmatrix} -1.3613 \\ 0.7972 \\ 2.5681 \\ 0.0199 \\ -0.5968 \\ -1.2367 \end{bmatrix}$$

As soon as we get the coefficients P for Landsat 8 OLI, we can calculate the pattern decomposition coefficients (C_w, C_v, C_s, C_4) by using the least square method principle. Lastly, we obtained single Landsat 8 image was used to calculate VIUPD and NDVI respectively.

4. RESULTS AND DISCUSSION

Figure 1 describes a standard vegetation pixel in the Landsat image value change during the atmospheric correction. It is proved that 6S methodology can reduce the atmosphere effect on the satellite data. For example, the Rayleigh scattering in the blue band has been greatly modified.

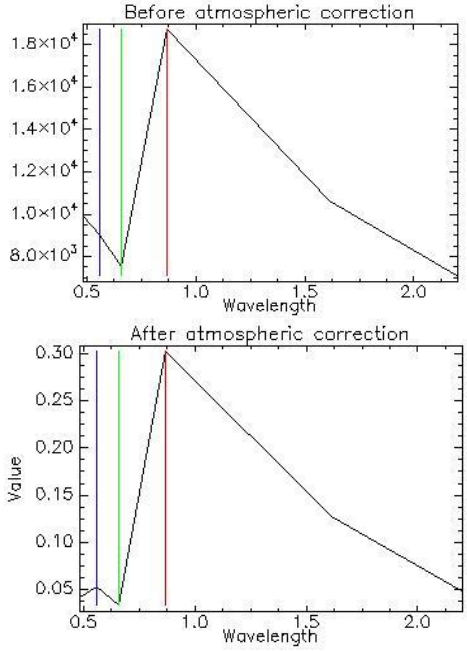

Figure 1. Value before and after atmospheric correction. Three lines stands for the false color display of the image. The upper figure is DN value, while the below figure is reflectance value.

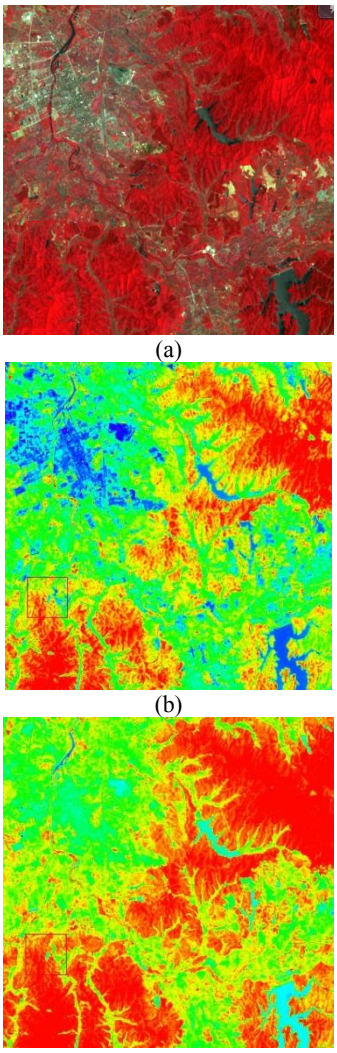

Figure 2. Subfigure (a) stands for the false color representation of the original Landsat 8 data; (b) stands for the result of VIUPD by standard rainbow color mapping; (c) stands for the result of NDVI by standard rainbow color mapping.

Once we get the reflectance data through radiometric calibration and atmospheric correction, we can easily calculate the NDVI using the band math. VIUPD can be got by firstly input the normalized reflectance (P) of standard samples which are the water, vegetation, soil and supplementary yellow leaf. Then calculate the pattern decomposition coefficients (C). In the end, get VIUPD according to equation 7. Figure 2 is the display of vegetation indices calculate from the processed Landsat data. From the images, we can tell that it is earlier for NDVI to reach saturation than VIUPD especially on the high vegetation coverage area. Although the ratio concept of NDVI will reduce many forms of multiplicative noise such as illumination differences, cloud shadows, atmospheric attenuation and certain topographic variations [13-15], the linear stretch will make the NDVI easily saturation in high vegetation coverage. On the other hand, VIUPD

distinguishes the urban and vegetation area better than NDVI which presents VIUPD more sensitive to the land cover change.

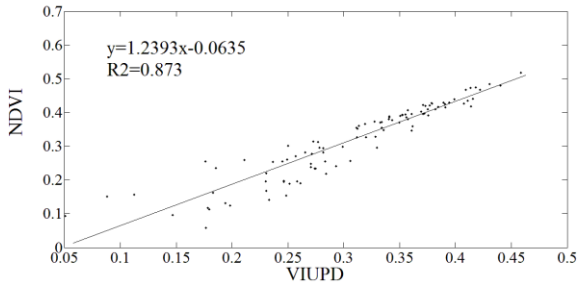

Figure 3. The correlation relationship between VIUPD and NDVI.

In order to quantitative analysis, we generate 100 random pixels from the region of interest of displayed figure 2. The correlation relationship between VIUPD and NDVI is expressed in figure 3. The X axis stands for the VIUPD value, while the Y axis stands for the NDVI value of the same 100 pixels. Generally, NDVI values are greater than VIUPD since the slope is 1.2393 which is greater than 1. Relevance represented by R^2 =0.873 show the high correlation between VIUPD and NDVI.

5. CONCLUSIONS

Landsat series historical sensors (TM, ETM+) have been used to construct vegetation index based on the universal pattern decomposition method (VIUPD) and achieved good application effect. This is the first time that the VIUPD been applied on the Landsat new sensor—Operational Land Imager (OLI) on board Landsat 8.

VIUPD can provide sensor-independent values and enables direct comparisons using remote sensing data from various sources. This advantageous will be really helpful for the long-term observation data comparison.

6. ACKNOWLEDGEMENT

This research is jointly sponsored by the National Natural Science Foundation of China (Project Numbers 41371362, 41201348, and 41202234).

7. REFERENCES

[1] R. D. Jackson and A. R. Huete, "Interpreting vegetation indices," *Preventive Veterinary Medicine,* vol. 11, pp. 185-200, 1991.

[2] L. Zhang, N. Fujiwara, S. Furumi, K. Muramatsu, M. Daigo, and L. Zhang, "Assessment of the universal pattern decomposition method using MODIS and ETM+ data," *International Journal of Remote Sensing,* vol. 28, pp. 125-142, 2007.

[3] X. Chen, L. Zhang, X. Zhang, and B. Liu, "Comparison of the sensor dependence of vegetation indices based on Hyperion and CHRIS hyperspectral data," *International Journal of Remote Sensing,* vol. 34, pp. 2200-2215, 2013.

[4] T. Arvidsona, J. Gaschb, and S. N. Gowardc, "Landsat 7's long-term acquisition plan — an innovative approach to building a global imagery archive," *Remote Sensing of Environment,* 2001.

[5] M. A. Wulder, J. C. White, S. N. Goward, J. G. Masek, J. R. Irons, M. Herold*, et al.*, "Landsat continuity: Issues and opportunities for land cover monitoring," *Remote Sensing of Environment,* vol. 112, pp. 955-969, 2008.

[6] W. B. Cohen, Z. Yang, and R. Kennedy, "Detecting trends in forest disturbance and recovery using yearly Landsat time series: 2. TimeSync — Tools for calibration and validation," *Remote Sensing of Environment,* vol. 114, pp. 2911-2924, 2010.

[7] E. K. Melaas, M. A. Friedl, and Z. Zhu, "Detecting interannual variation in deciduous broadleaf forest phenology using Landsat TM/ETM+ data," *Remote Sensing of Environment,* vol. 132, pp. 176-185, 2013.

[8] R. H. Fraser, I. Olthof, M. Carrière, A. Deschamps, and D. Pouliot, "Detecting long-term changes to vegetation in northern Canada using the Landsat satellite image archive," *Environmental Research Letters,* vol. 6, p. 045502, 2011.

[9] J. G. Masek, F. E. Lindsay, and S. N. Goward, "Dynamics of urban growth in the Washington DC metropolitan area, 1973-1996, from Landsat observations," *International Journal of Remote Sensing,* vol. 21, pp. 3473-3486, 2000.

[10] L. Zhang, S. Furumi, K. Muramatsu, N. Fujiwara, M. Daigo, and L. Zhang, "Sensor‐independent analysis method for hyperspectral data based on the pattern decomposition method," *International Journal of Remote Sensing,* vol. 27, pp. 4899-4910, 2006.

[11] E. F. Vermote, N. El Saleous, C. O. Justice, Y. J. Kaufman, J. L. Privette, L. Remer*, et al.*, "Atmospheric correction of visible to middle-infrared EOS-MODIS data over land surfaces: Background, operational algorithm and validation," *Journal of Geophysical Research,* vol. 102, p. 17131, 1997.

[12] J. G. Masek, E. F. Vermote, N. E. Saleous, R. Wolfe, F. G. Hall, K. F. Huemmrich*, et al.*, "A Landsat Surface Reflectance Datasetfor North America, 1990-2000," *IEEE GEOSCIENCE AND REMOTE SENSING LETTERS,* vol. 3, pp. 68-72, 2006.

[13] A. Huete, K. Didan, T. Miura, E. P. Rodriguez, X. Gao, and L. G. Ferreira, "Overview of the radiometric and biophysical performance of the MODIS vegetation indices," *Remote Sensing of Environment,* 2002.

[14] N. Pettorelli, J. O. Vik, A. Mysterud, J. M. Gaillard, C. J. Tucker, and N. C. Stenseth, "Using the satellite-derived NDVI to assess ecological responses to environmental change," *Trends Ecol Evol,* vol. 20, pp. 503-10, Sep 2005.

[15] A. Tittebrand, U. Spank, and C. H. Bernhofer, "Comparison of satellite- and ground-based NDVI above different land-use types," *Theoretical and Applied Climatology,* vol. 98, pp. 171-186, 2009.